JOINT IMAGE DENOISING USING SELF-SIMILARITY BASED LOW-RANK APPROXIMATIONS

Yongqin Zhang, Jiaying Liu, Saboya Yang, Zongming Guo*

Institute of Computer Science and Technology, Peking University, Beijing 100871, China

ABSTRACT

The observed images are usually noisy due to data acquisition and transmission process. Therefore, image denoising is a necessary procedure prior to post-processing applications. The proposed algorithm exploits the self-similarity based low rank technique to approximate the real-world image in the multivariate analysis sense. It consists of two successive steps: adaptive dimensionality reduction of similar patch groups, and the collaborative filtering. For each target patch, the singular value decomposition (SVD) is used to factorize the similar patch group collected in a local search window by block-matching. Parallel analysis automatically selects the principal signal components by discarding the nonsignificant singular values. After the inverse SVD transform, the denoised image is reconstructed by the weighted averaging approach. Finally, the collaborative Wiener filtering is applied to further remove the noise. Experimental results show that the proposed algorithm surpasses the state-of-the-art methods in most cases.

Index Terms— Dimensionality reduction, parallel analysis, eigenvalue decomposition, low-rank approximation

1 Introduction

The scene captured in data acquisition is often a single image or multiple images deteriorated by various noise sources. Consequently, image denoising has become a key focus of ongoing studies in recent years. The goal of image denoising is to reconstruct a high-quality signal from its noise-corrupted observation. As it is a typically ill-posed inverse problem, the solution is generally not unique. To find a better solution, many powerful methods have appeared over the past several years for image denoising. After a brief review, there are two basic categories for image denoising algorithms. One category is the spatial filters, which can be further classified into linear filters and non-linear filters. Some recent popular linear spatial filters are NLM (Nonlocal Means filter) [1, 2, 3], and TLS (Total Least Squares) [4]. The other category is transforming domain filtering methods, which also can be further divided into the non-data adaptive transform including wavelet-based variants, and the data adaptive transform, such as, K-SVD [5], BM3D [7], and PCA [8, 9]. The patch-based PLPCA method [9] employs the hard thresholding technique directly applied on the elements of the eigenvectors, whereas it also damages the sharp edges and the fine structures. However, its thresholding value is based on the known noise deviation. In fact, the noise deviation is unknown in most cases. The existing best state-of-the-art filtering methods are mostly based on the optimal Wiener filter [7] or equivalently Linear-Minimum Mean Squared Error (LMMSE) [8]. Although they have very good performance for reducing additive white Gaussian noise (AWGN) from the noisy image, they have not yet reached the limit of noise removal [11].

It is found that the patch-based techniques based on global basis or dictionary can provide efficient representations for global features, while the data-driven local bases have the potential to capture local structures and details. As yet, their difficulties have existed in finding suitable training samples as well as choosing the proper signal components. Similar to the framework of BM3D [7], in this paper, we propose the joint denoising algorithm consisting of two successive steps: the self-similarity based low-rank approximation, and the empirical Wiener filtering. Our main contributions of the proposed algorithm include both the combined denoising strategy, and adaptive dimensionality reduction approach of similar patch groups by parallel analysis. The experimental results show that the proposed algorithm achieves a state-of-the-art denoising performance, and outperforms recently published leading alternative denoising methods in most cases from subjective and objective measures of image quality.

The rest of this paper is organized as follows. In Section 2, we briefly review the related concepts, and describe the proposed joint denoising algorithm using the self-similarity based low-rank approximations. Section 3 shows the simulation and experimental results of the developed algorithm as compared to the state-of-the-arts methods. The discussions and conclusions are given in Section 4.

∗ Corresponding author

This work was supported by National Natural Science Foundation of China under contract No.61201442, National Key Technology R&D Program of China under Grant 2012BAH18B03 and China Postdoctoral Science Foundation funded project under contract No.2013M530481.

2 The Proposed Algorithm

In real-world digital-imaging devices, the acquired images are often corrupted by device-specific noise. A simplified model of an independent additive noise usually used to denote the degradation process of the noisy images is given in this formula [1, 10]:

$$y(x) = s(x) + \upsilon(x) \tag{1}$$

where x is the coordinate; y is the observed image, s is the clean image, and υ represents additive noise source, such as Gaussian noise.

2.1 Image Patch Clustering

Since each patch contains a pixel and its nearest neighbors that can better preserve edge structures and texture patterns, the patch-based image representation is modeled instead of the pixel-based image for noise reduction. For an observed noisy image $\mathbf{Y}$ with its coordinate domain $\mathbf{X} \subset \mathbf{R}^{M\times N}$, let $y(x)$ be a pixel at a position x in the image $\mathbf{Y}$. The patch-based image $\mathbf{Y}_x$ denotes a patch of fixed size $\sqrt{P}\times\sqrt{P}$ extracted from $\mathbf{Y}$, where x is the coordinate of the central pixel of the patch. That is, $\mathbf{Y}_x$ is a reshaped vector of size $P\times 1$, which contains the $\sqrt{P}\times\sqrt{P}$ pixels consisting of a central pixel $y(x)$ and its nearest neighbors in the observed image $\mathbf{Y}$.

For each target pixel $y(x)$ located in the central position of the target patch $\mathbf{Y}_x$, there are totally L possible training patches of the same size $\sqrt{P}\times\sqrt{P}$ in the $\sqrt{L}\times\sqrt{L}$ local search window. However, there may be very different adjacent patches from the given target patch so that taking all the $\sqrt{L}\times\sqrt{L}$ patches as the training samples will cause inaccurate estimation of the target patch vector $\mathbf{Y}_x$. As is known to all, the high degree of self-similarity and redundancy exists within any natural image. Thus, it's necessary to choose and cluster the training samples that are similar to the target patch for the full use of both local and nonlocal information. Then, the data-adaptive SVD transform is used to separate the image signal and the noise from the similar patch groups. The problem of patch classification has several different solutions, *e.g.*, block matching [7] and K-means clustering [6]. For simplicity, we employ the block matching algorithm for image patch clustering.

For each target patch $\mathbf{Y}_x$, the block matching algorithm chooses L_s similar patches of the same size $\sqrt{P}\times\sqrt{P}$ in the $\sqrt{L}\times\sqrt{L}$ search window Ψ_x. The relationships between the central pixel, the target patch, the adjacent patch and the local search window are described in Figure 1. The similarity measurement between the adjacent patch and the target patch can be calculated based on Euclidean distance in this formula:

$$e_l = \frac{1}{P}\sum_{p=1}^{P}\left(y_l(p) - y_x(p)\right)^2 \tag{2}$$

where $l = 1, 2, \cdots, L$. After the error vector $\mathbf{e} = [e_1, \cdots, e_L]^T$ is sorted in the ascending order, the top most similar patches are chosen to construct the patch group. Assume that we select L_s similar patch vectors to reconstruct the patch group $\mathbf{Z}_x^\upsilon$ for the target patch $\mathbf{Y}_x$, where L_s is a preset number. For each target patch $\mathbf{Y}_x$, the patch group $\mathbf{Z}_x^\upsilon$ consisting of the training patches can be expressed in this form:

$$\mathbf{Z}_x^\upsilon = [\mathbf{Y}_x, \mathbf{Y}_1, \cdots, \mathbf{Y}_{L_s-1}]^T \tag{3}$$

To separate the image signal and the noise effectively, the number L_s of most similar patches should be large enough. The patch clustering matrix $\mathbf{Z}_x^\upsilon$ or its transposition $(\mathbf{Z}_x^\upsilon)^T$ will be used to avoid the problem of rank deficiency in computing the SVD of the covariance matrix of $\mathbf{Z}_x^\upsilon$. For each noisy measurement $\mathbf{Z}_x^\upsilon$, the next procedure is to estimate its underlying noiseless counterpart dataset $\mathbf{Z}_x = [\mathbf{S}_x, \mathbf{S}_1, \cdots, \mathbf{S}_{L_s-1}]^T$.

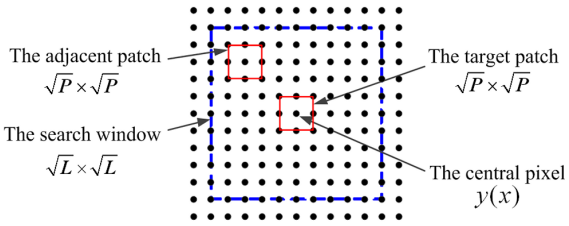

Fig. 1: The relationships between the central pixel, the target patch, the adjacent patch and the local search window.

2.2 Adaptive Dimensionality Reduction

After singular value decomposition (SVD) of noisy image data, it's observed that most of image signal is mainly concentrated on the top several principal components, whereas the eigenvectors of the small singular values are almost all noises. The denoising problem of the noisy patch group $\mathbf{Z}_x^\upsilon$ is indeed how to select the optimal number of the principal components in the SVD transform domain. In this paper, we employ dimensionality reduction technique to analyze the eigenvalues of the covariance matrix of the patch group $\mathbf{Z}_x^\upsilon$. By subtracting the sample mean value from each column, we have computed the zero-centered matrix from the patch group $\mathbf{Z}_x^\upsilon$ in this formula:

$$\bar{Z}_x^\upsilon(l,p) = Z_x^\upsilon(l,p) - M_x(l,p) \tag{4}$$

where $M_x(l,p) = [1,\cdots,1]^T \times \frac{1}{L_s}\sum_{l=1}^{L_s} Z_x^\upsilon(l,p)$; $[1,\cdots,1]^T$ is the column vector of size $L_s\times 1$; $l = 1,\cdots,L_s$; and $p = 1,\cdots,P$.

To reduce calculation time in an efficient way, the covariance matrix $\left(\bar{\mathbf{Z}}_x^\upsilon\right)^T\bar{\mathbf{Z}}_x^\upsilon$ instead of the zero-centered patch group $\bar{\mathbf{Z}}_x^\upsilon$ is used to be factorized in this form:

$$\left(\bar{\mathbf{Z}}_x^\upsilon\right)^T\bar{\mathbf{Z}}_x^\upsilon = \mathbf{V}\mathbf{\Sigma}^2\mathbf{V}^T \tag{5}$$

where the symbol T denotes the transpose operator, and $\mathbf{V}$ is the unitary matrix of eigenvectors derived from $\left(\bar{\mathbf{Z}}_x^v\right)^T \bar{\mathbf{Z}}_x^v$. Σ is a $P \times P$ diagonal matrix with its singular values $\lambda_1 \geq \lambda_2 \geq \cdots \geq \lambda_r \geq 0$ and $r = \mathrm{rank}\left(\bar{\mathbf{Z}}_x^v\right)$.

In fact, the eigenvalues of the covariance matrix of the noise v are not the same constant. Therefore, we can not take a preset fixed threshold to select the signal components. As we know, if the eigenvalues are very small and the size of the image patch from a single noisy image is large enough, the discard of less significant components does not lose much information. From the diagonal singular values, only the first K primary eigenvectors are retained based on dimensionality reduction techniques. However, the parameter K should be not only large enough to allow fitting the characteristics of the data, but also small enough to filter out the non-relevant noise and redundancy. There are various dimensionality reduction methods proposed in the literatures for determining the number of components to retain in data analysis. The parallel analysis (PA) method firstly introduced by Horn [12, 13] compares the observed eigenvalues to be analyzed with those of an artificial data set. It proves that PA is one of the most successful methods for determining the number of true principal components. In this paper, we adopt the proposed parallel analysis with Monte Carlo simulation to choose the top K largest values.

Let λ_p for $p = 1, \cdots, P$ denote the singular values of the zero-centered patch group $\bar{\mathbf{Z}}_x^v$ sorted in the descending order. Similarly, let α_p denote the sorted singular values of the artificial data. Therefore, the proposed parallel analysis estimates the number of signal components in noisy data as follows:

$$K = \max\left\{p = 1, \cdots, P | \lambda_p \geq \alpha_p\right\} \tag{6}$$

Currently, it is recommended to use the singular value that corresponds to a given percentile, such as the 95^{th} of the distribution of singular values derived from the random data set. In our algorithm, without any assumption of a given random distribution, we generate the artificial data by randomly permuting each element of all the patch vectors located in a search window. Then singular values of the random artificial data are computed by the SVD transform. For the L_s by P synthetic matrix $\mathbf{C_s}$, after multiple times (*e.g.* 10) of Monte Carlo simulations, summary statistics (*e.g.* 95^{th} percentile) can be used to extract the P singular values α_p in the descending order. Then parallel analysis is applied and the two lines denote singular values of the simulated data $\mathbf{C_s}$ and the zero-centered patch group $\bar{\mathbf{Z}}_x^v$, respectively. The intersection of the two lines is the cutoff for determining the number of the signal components presented in the noisy image.

While the traditional principal component analysis (PCA) [14] takes the thresholding technique to estimate data dimensionality, the proposed adaptive PCA approach can automatically determine signal subspace dimensions in noisy data by the parallel analysis technique. Our developed refined parallel analysis using Monte Carlo simulation, and the traditional PCA [14] were compared for dimensionality reduction in our experiments. Suppose that a 25×25 fragment of *lena* image corrupted by additive zero-mean Gaussian noise with standard deviation 20. In this case, the signal dimensionality of the given noisy patch group $\mathbf{Z}_x^v$ with patch size 5×5 pixels was separately estimated by the proposed adaptive PCA and the traditional PCA [14]. Figure 2 shows the numbers of its signal components estimated by the proposed adaptive PCA technique, and the traditional PCA [14] are separately 5, and 19. We can see that the proposed adaptive PCA approach is better than the traditional PCA method for separating the signal and the noise from the noisy image.

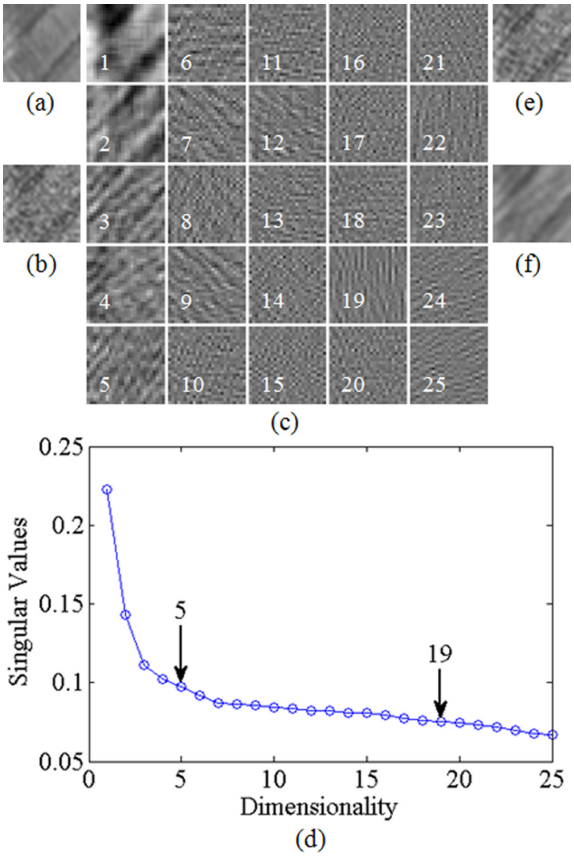

Fig. 2: The eigenimages, the singular values, and the reconstructed images generated from a 25×25 image block with patch size 5×5 pixels of the test *lena* image corrupted by additive zero-mean Gaussian noise with standard deviation 20. (a) the original image block; (b) the noisy image block; (c) the eigenimages; (d) the numbers of its signal subspace dimensionality estimated by the proposed adaptive PCA approach, and the traditional PCA [14] are 5, and 19,respectively; (e) the reconstructed image block ($K = 19$); (f) the reconstructed image block ($K = 5$).

2.3 SVD-Based Low-Rank Approximation

For each target pixel $y(x)$, the similar candidate patches are selected by the block matching algorithm to constitute the patch group $\mathbf{Z}_x^v = [\mathbf{Y}_x, \mathbf{Y}_1, \cdots, \mathbf{Y}_{L_s-1}]^T$. The patch-based correlated patch groups $\mathbf{Z}_x^v$ $(x \in \mathbf{X})$ [see (3)] can be used for component analysis of the noisy image $\mathbf{Y}$. The low-rank approximation [15, 16] is used to estimate the original noiseless image $\mathbf{S}$ by reducing noise of the observed image $\mathbf{Y}$. Therefore, the zero-centered patch group $\bar{\mathbf{Z}}_x^v$ is factorized by the SVD transform in this formula:

$$\bar{\mathbf{Z}}_x^v = \mathbf{U}\Sigma\mathbf{V}^T \tag{7}$$

where Σ is the diagonal matrix with the singular values $\lambda_1 \geq \lambda_2 \geq \cdots \geq \lambda_r$. $\mathbf{V} = [\mathbf{V}_1, \mathbf{V}_2, \cdots, \mathbf{V}_P]$ and $\mathbf{U} = [\mathbf{U}_1, \mathbf{U}_2, \cdots, \mathbf{U}_{L_s}]$ are the unitary matrices of eigenvectors, which represent the orthogonal dictionaries of nonlocal bases and local bases, respectively. The zero-centered noisy patch group $\bar{\mathbf{Z}}_x^v$ is decomposed into a sum of components from the largest to the smallest singular values. In fact, most of the energy of the true image is concentrated on few high-magnitude transform coefficients, whereas the corresponding eigenimages of the small singular values are almost all noises.

After adaptively determining the signal dimension of the noisy zero-centered patch groups $\bar{\mathbf{Z}}_x^v$ [see (6)], the denoised image can be reconstructed by the SVD-based low rank approach. The straightforward way to restore a noiseless image is to directly apply the inverse SVD transform to the noisy similar patch groups $\mathbf{Z}_x^v$ in a reduced dimensionality representation. That is, the inverse SVD transform is implemented to approximate the true noise-free image with the matrices $\mathbf{\Sigma}_K = \operatorname{diag}\{\lambda_1, \lambda_2, \cdots, \lambda_K\}$, $\mathbf{U}_K = [\mathbf{U}_1, \mathbf{U}_2, \cdots, \mathbf{U}_K]$, and $\mathbf{V}_K = [\mathbf{V}_1, \mathbf{V}_2, \cdots, \mathbf{V}_K]$. For each target pixel, the denoised patch group $\hat{\mathbf{Z}}_x$ and its weight matrix $\mathbf{W}_x$ are separately estimated as follows:

$$\hat{\mathbf{Z}}_x = \mathbf{U}_K\mathbf{\Sigma}_K\mathbf{V}_K^T + \mathbf{M}_x \tag{8}$$

$$W_x(l,p) = \begin{cases} 1 - K/P, K < P; \\ 1/P, \qquad K = P. \end{cases} \tag{9}$$

where $\mathbf{M}_x$ is the mean value [see (4)] of the patch group $\mathbf{Z}_x^v$.

After applying such procedures to each pixel $y(x)$, the relevant denoised patch group is estimated according to Equation (8), and its weight is empirically determined in Equation (9). Since these denoised patches are overlapping, multiple estimates of each pixel in the image are combined to reconstruct the whole image. The weighted averaging procedure is carried out to suppress the noise further. The whole filtered image $\hat{\mathbf{S}}^t$ is obtained by aggregating all the estimates of each pixel in this formula:

$$\hat{\mathbf{S}}^t = \frac{1}{\mathbf{W}^t} \sum_{x=1}^{M\times N} \hat{\mathbf{Z}}_x \mathbf{W}_x \tag{10}$$

where the total weight $\mathbf{W}^t = \sum_{x=1}^{M\times N} \mathbf{W}_x$.

Moreover, the proposed efficient algorithm is implemented by reducing the number of the image patch groups. A step of $J_s \in X$ pixels is used for the noisy image in both horizontal and vertical directions. Thus, the number of similar patch groups is approximately MN/J_s^2 rather than MN. Hence most of the noise will be removed by using the adaptive dimensionality reduction approach and the weighted averaging scheme in Sections 2.2-2.4. However, there is still some unpleasant residual noise in the denoised image, especially for terribly noisy images. As the observed image contains the strong noise, the image patches are seriously corrupted by noise, which leads to image patch clustering errors and the biased estimation of the SVD transform. Consequently, it is necessary to further suppress the noise residual of the denoised output $\hat{\mathbf{S}}^t$.

After the first phase of noise removal by the low rank approximation, the empirical Wiener filtering [7] is employed for the second phase to further improve the denoising performance of the output $\hat{\mathbf{S}}^t$. Because there is less noise in the output $\hat{\mathbf{S}}^t$, the close approximation of the true patch distance is calculated with the denoised output $\hat{\mathbf{S}}^t$ instead of the noisy image $\mathbf{Y}$ [see (2)]. Therefore, the final whole noiseless image $\hat{\mathbf{S}}^f$ is obtained after the empirical Wiener filtering. In addition, the pseudo codes of **Algorithm** 1 gives further clarification of the proposed denoising algorithm.

3 RESULTS AND ANALYSIS

The qualitative and quantitative evaluation of the proposed algorithm was implemented on lots of test benchmark images including *Lena*, *Baboon*, *Barbara*, *House* and *brain* from standard image databases [18]. To perform a quantitative comparison between the performances of the proposed denoising algorithm and the state-of-the-art methods published recently [7, 9], the two well-known noise-reduction full reference quality metrics: PSNR (Peak Signal to Noise Ratio) and SSIM (Structural SIMilarity) [17] are considered for measuring the similarity between the denoised image and original noise-free image. In this experiment, the test images were degraded by additive Gaussian noise with zero means and different deviations 10, 20, 30 and 50 respectively. The performance of our developing algorithm was compared with the current state-of-the-art methods, such as BM3D [7] and PLPCA [9]. The PSNR results for five test images are presented in Table 1. The detailed visual results for the proposed algorithm, BM3D [7] and PLPCA [9] for the fragments of

Algorithm 1 Pseudocode of the Proposed Algorithm

Input: $\mathbf{Y}^{M\times N}$, P, L and L_s.
Output: $\hat{\mathbf{S}}^f$

for each $x = 1$ to $M \times N$ **do**
  for each $i, j = 1$ to $\sqrt{P}$ **do**
    $p = (i-1) \times \sqrt{P} + j$;
    $H(x,p) = Y\left(m + i - \sqrt{P}, n + j - \sqrt{P}\right)$;
  end for
end for
$\hat{S}^t = \text{zeros}(M \times N, P)$; $W^t = \text{zeros}(M \times N, P)$;
for each $x = 1$ to $M \times N$ **do**
  $\Psi_x \leftarrow L$; $Y_x = H(x,:)$; $Y_{\Psi_x} = H(\Psi_x,:)$;
  $\Psi_x^s = \text{BlockMatching}(Y_x, Y_{\Psi_x}, L_s)$;
  $Z_x^\upsilon = H(\Psi_x^s,:)$; $M_x = \text{mean}(Z_x^\upsilon)$;
  $\bar{Z}_x^\upsilon = Z_x^\upsilon - M_x$; $\left(\bar{Z}_x^\upsilon\right)^T \bar{Z}_x^\upsilon = V\Sigma^2 V^T$;
  $C^T C = V\Lambda^2 V^T$;
  $\lambda = \text{diag}(\Sigma)$; $\alpha = \text{diag}(\Lambda)$;
  $K = \max\{p = 1, \cdots, P | \lambda_p \geq \alpha_p\}$;
  $\hat{Z}_x = U_K \Sigma_K V_K^T + M_x$;
  $\hat{S}^t(\Psi_x^s,:) = \hat{S}^t(\Psi_x^s,:) + W_x \hat{Z}_x$;
  $W^t(\Psi_x^s,:) = W^t(\Psi_x^s,:) + W_x$;
end for
$I = \text{zeros}\left(M + \sqrt{P} - 1, N + \sqrt{P} - 1\right)$;
$Q = \text{zeros}\left(M + \sqrt{P} - 1, N + \sqrt{P} - 1\right)$;
for each $a, b = 1$ to $\sqrt{P}$ **do**
  $id = (b-1) \times \sqrt{P} + a$;
  $\Pi_a = a : M + a - 1$; $\Pi_b = b : N + b - 1$;
  $T_S = \text{reshape}\left(\hat{S}^t(:, id), [M, N]\right)$;
  $I(\Pi_a, \Pi_b) = I(\Pi_a, \Pi_b) + T_S$;
  $T_W = \text{reshape}(W_t(:, id), [M, N])$;
  $Q(\Pi_a, \Pi_b) = Q(\Pi_a, \Pi_b) + T_W$;
end for
$\hat{S}^t = I/Q$;
$\hat{S}^f = \text{WienerFiltering}\left(\hat{S}^t\right)$;

the *Lena*, and *Barbara* images are shown in from Figure 3 to Figure 4. Further, our adaptive dimensionality reduction approach can discard considerable part of noises almost without loss of signal information.

Besides this set of experiments on the simulated noisy images, we also validate our denoising algorithm on real magnetic resonance (MR) images acquired from the MR scanner at 3T (MAGNETOM Tim Trio, Siemens, Germany). They were scanned with the pulse sequences including spin echo (SE) in the study. The *T1_SE* image provides a testing set which presents a good diversity: different organs (White matter/Grey matter). Figure 5 presents the results for the different real MR images and different denoising methods. These experiments verify that the proposed algorithm can be effectively applied to real MR images. It is evident that the proposed algorithm achieves a better edge and structure preservation. As seen from the experimental results of both synthetic Images and real MR images, the proposed algorithm can reach better results than other state-of-the-art methods in most cases. Moreover, it works well for a wide variety of noisy images and also has better noise reduction effect, especially on regions of rich textures and edges.

Table 1: The final PSNR(dB) results of the restored images obtained by these different denoising methods for test images with different noise levels. The values in parenthesis are the PSNR results of the first stage in the corresponding denoising methods. For each image, the three rows correspond to the noise standard deviation 10, 20, 30, and 50, respectively.

Images	[7]	[9]	Proposed
Lena 512×512	**(35.67)35.94**	35.54	(35.28)**35.94**
	(32.47)33.00	32.32	(32.03)32.91
	(30.47)31.20	30.26	**(30.53)31.33**
	(27.77)28.74	27.21	**(27.78)28.86**
Baboon 512×512	(30.74)30.96	**31.08**	(29.33)30.62
	(26.79)27.15	27.03	**(26.94)27.28**
	(24.89)25.20	25.04	**(25.24)25.42**
	(22.82)23.13	23.01	**(23.17)23.46**
Barbara 512×512	(34.62)34.96	34.75	**(34.63)35.18**
	(31.16)31.75	31.08	**(31.34)31.86**
	(28.86)29.74	28.89	**(29.61)30.10**
	(25.77)27.21	25.98	**(26.46)27.54**
House 256×256	**(36.27)**36.69	35.78	(35.83)**36.72**
	(33.47)33.90	32.61	(32.78)33.87
	(31.41)32.09	30.46	(31.18)**32.10**
	(28.50)29.80	27.21	**(28.65)29.86**
Brain 256×256	**(33.58)33.75**	33.61	(33.09)33.66
	(29.97)30.24	29.57	(29.49)**30.38**
	(27.66)28.04	27.13	**(27.78)28.26**
	(24.74)25.33	24.47	**(24.95)25.65**

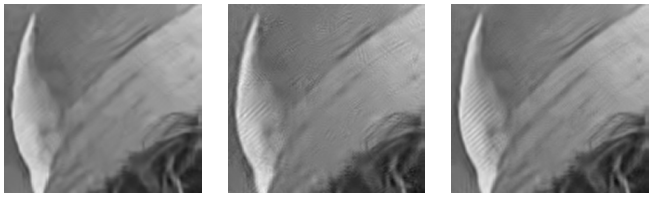

(a) (b) (c)

Fig. 3: Visual comparisons of the denoising results for the *Lena* image corrupted with Gaussian noise with standard deviation 30. From left to right: (a) BM3D [7] (PSNR=31.20dB, SSIM=.8440); (b) PLPCA [9] (PSNR=30.26dB, SSIM=.7956); and (c) Proposed (PSNR=31.33dB, SSIM=.8424).

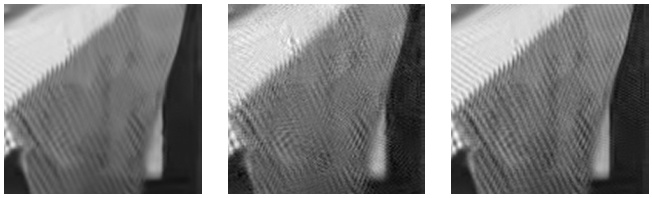

(a) (b) (c)

Fig. 4: Visual comparisons of the denoising results for the *Barbara* image corrupted with Gaussian noise with standard deviation 50. From left to right: (a) BM3D [7] (PSNR=27.21dB, SSIM=.7928); (b) PLPCA [9] (PSNR=25.98dB, SSIM=.6792); and (d) Proposed (PSNR=27.54dB, SSIM=.8014).

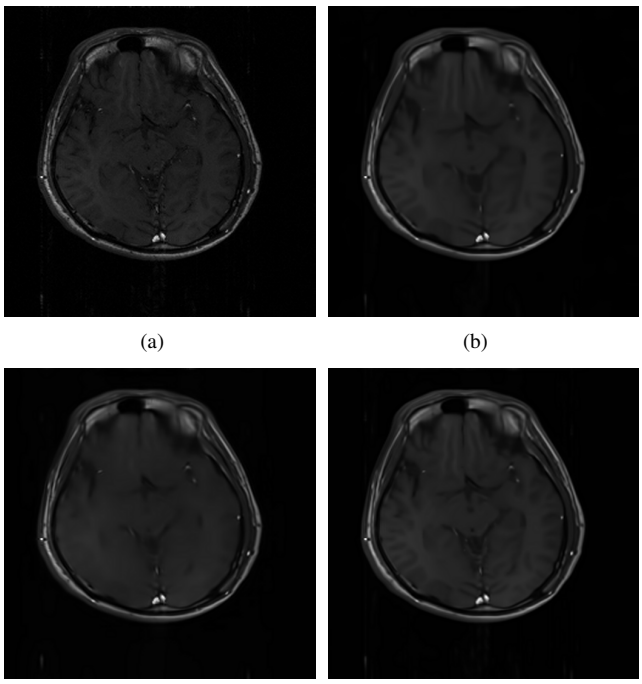

(a) (b)

(c) (d)

Fig. 5: Visual comparisons of the denoising results for the *T1_SE* image. (a) Noisy MR image; (b) BM3D [7]; (c) PLPCA [9]; and (d) Proposed.

4 CONCLUSIONS

In this paper, we addressed the joint denoising framework using the self-similarity based low-rank approximation. Parallel analysis adaptively selects the proper signal components of similar patch groups from the noisy images. Thus this dimensionality reduction approach discards a considerable part of noises almost without loss of signal information. Then the inverse SVD transform, whose left and right orthogonal basis denote local and nonlocal image features, respectively, is implemented to obtain the first-stage denoised image by the weighted averaging aggregation operator. After applying the empirical Wiener filtering to the first-stage denoised image, the reconstructed noise-free image is achieved with better denoising performance. The results of test images corrupted with variant noise levels demonstrate that the proposed joint denoising algorithm is better than the state-of-the-art methods both visually and quantitatively in most cases.

5 References

[1] A. Buades, B. Coll, and J. M. Morel. A Review of Image Denoising Algorithms, with a New One. *Multiscale Model. Simul.*, 4(2):490-530, 2005.

[2] T. Tasdizen. Principal Neighborhood Dictionaries for Non-local Means Image Denoising. *IEEE Trans. Image Process.*, 18(12):2649-2260, 2009.

[3] D. van de Ville and M. Kocher. SURE-Based non-local means. *IEEE Signal Process Lett.*, 16(11):973-976, 2009.

[4] K. Hirakawa, and T. W. Parks. Image Denoising using Total Least Squares. *IEEE Trans. Image Process.*, 15(9):2730-2742, 2006.

[5] M. Aharon, M. Elad, and A. M. Bruckstein. K-SVD: An Algorithm for Designing of Overcomplete Dictionaries for Sparse Representation. *IEEE Trans. Image Process.*, 54(11):4311-4322, 2006.

[6] R. C. Amorim, and B. Mirkin, Minkowski metric. Feature weighting and anomalous cluster initializing in K-Means clustering. *Pattern Recognit.*, 45(3):1061-1075, 2012.

[7] K. Dabov, A. Foi, V. Katkovnik, and K. Egiazarian, Image Denoising by Sparse 3D Transform-Domain Collaborative Filtering, *IEEE Trans. Image Process.*, 16(8):2080-2095, 2007.

[8] L. Zhang, W. Dong, D. Zhang, and G. Shi. Two-stage image denoising by principal component analysis with local pixel grouping. *Pattern Recognit.*, 43(4):1531-1549, 2010.

[9] C. A. Deledalle, J. Salmon, A. S. Dalalyan. Image denoising with patch based PCA: local versus global. *Proceedings of BMVC*, Dundee, Scotland, Aug.29 -Sep.2, 2011.

[10] H. Takeda, S. Farsiu, and P. Milanfar. Kernel Regression for Image Processing and Reconstruction. *IEEE Trans. Image Process.*, 16(2):349-366, 2007.

[11] P. Chatterjee, and P. Milanfar. Is Denoising Dead?. *IEEE Trans. Image Process.*, 19(4):895-911, 2010.

[12] J. L. Horn. A rationale and test for the number of factors in factor analysis. *Psychomerica*, 30(2):179-185, 1965.

[13] K. W. Jorgensen, and L. K. Hansen. Model Selection for Gaussian Kernel PCA Denoising. *IEEE Trans. Neural Netw. Learn. Syst.*, 23(1):163-168, 2012.

[14] L.J.P. van der Maaten, E.O. Postma, and H.J. van den Herik. Dimensionality Reduction: A Comparative Review. *Tilburg University Technical Report*, TiCC-TR:2009-005, 2009.

[15] Siep Weiland, and Femke van Belzen. Singular Value Decompositions and Low Rank Approximations of Tensors. *IEEE Trans. Image Process.*, 58(3):1171-1182, 2010.

[16] I. Markovsky. Low-Rank Approximation: Algorithms, Implementation, Applications. *Springer*, 2012.

[17] Z. Wang, A. C. Bovik, H. R. Sheikh and E. P. Simoncelli. Image quality assessment: From error visibility to structural similarity. *IEEE Trans. Image Process.*, 131(4):600-612, 2004.

[18] Image database, *http://decsai.ugr.es/cvg/dbimagenes/*, Mar.22, 2013.